Heralded Entanglement Between Widely Separated Atoms

Julian Hofmann *et al.*

Science **337**, 72 (2012);
DOI: 10.1126/science.1221856

5. E. Moraux, J. Bouvier, J. R. Stauffer, J.-C. Cuillandre, *Astron. Astrophys.* **400**, 891 (2003).
6. K. L. Luhman *et al.*, in *Protostars and Planets V*, B. Reipurth, D. Jewitt, K. Keil, Eds. (Univ. of Arizona Press, Tucson, AZ, 2007), pp. 443–457.
7. A. Whitworth, M. R. Bate, Å. Nordlund, B. Reipurth, H. Zinnecker, in *Protostars and Planets V*, B. Reipurth, D. Jewitt, K. Keil, Eds. (Univ. of Arizona Press, Tucson, AZ, 2007), pp. 459–476.
8. D. Ward-Thompson *et al.*, in *Protostars and Planets V*, B. Reipurth, D. Jewitt, K. Keil, Eds. (Univ. of Arizona Press, Tucson, AZ, 2007), pp. 33–46.
9. B. Reipurth, C. Clarke, *Astron. J.* **122**, 432 (2001).
10. M. R. Bate, I. A. Bonnell, V. Bromm, *Mon. Not. R. Astron. Soc.* **332**, L65 (2002).
11. I. Thies, P. Kroupa, S. P. Goodwin, D. Stamatellos, A. P. Whitworth, *Astrophys. J.* **717**, 577 (2010).
12. S. Basu, E. I. Vorobyov, *Astrophys. J.* **750**, 30 (2012).
13. A. P. Whitworth, H. Zinnecker, *Astron. Astrophys.* **427**, 299 (2004).
14. P. Padoan, Å. Nordlund, *Astrophys. J.* **576**, 870 (2002).
15. P. Hennebelle, G. Chabrier, *Astrophys. J.* **684**, 395 (2008).
16. R. B. Larson, *Mon. Not. R. Astron. Soc.* **214**, 379 (1985).
17. P. Padoan, Å. Nordlund, *Astrophys. J.* **617**, 559 (2004).
18. L. Loinard, R. M. Torres, A. J. Mioduszewski, L. F. Rodriguez, *Astrophys. J.* **675**, L29 (2008).
19. E. E. Mamajek, *Astron. Nachr.* **329**, 10 (2008).
20. M. W. Pound, L. Blitz, *Astrophys. J.* **444**, 270 (1995).
21. J. S. Greaves, W. S. Holland, M. W. Pound, *Mon. Not. R. Astron. Soc.* **346**, 441 (2003).
22. R. B. Loren, A. Wootten, B. A. Wilking, *Astrophys. J.* **365**, 269 (1990).
23. J. F. Alves, C. J. Lada, E. A. Lada, *Nature* **409**, 159 (2001).
24. L. Allen *et al.*, in *Protostars and Planets V*, B. Reipurth, D. Jewitt, K. Keil, Eds. (Univ. of Arizona Press, Tucson, AZ, 2007), pp. 361–376.
25. Ph. André *et al.*, *Astron. Astrophys.* **518**, L102 (2010).
26. A. P. Boss, H. W. Yorke, *Astrophys. J.* **439**, L55 (1995).
27. M. L. Enoch, J.-E. Lee, P. Harvey, M. M. Dunham, S. Schnee, *Astrophys. J.* **722**, L33 (2010).
28. R. Liseau *et al.*, *Astron. Astrophys.* **344**, 342 (1999).
29. D. Stamatellos, A. P. Whitworth, D. Ward-Thompson, *Mon. Not. R. Astron. Soc.* **379**, 1390 (2007).
30. F. Motte, P. André, R. Neri, *Astron. Astrophys.* **336**, 150 (1998).
31. J. M. Kirk, D. Ward-Thompson, P. André, *Mon. Not. R. Astron. Soc.* **360**, 1506 (2005).
32. F. Bertoldi, C. F. McKee, *Astrophys. J.* **395**, 140 (1992).

Acknowledgments: This work is based on observations carried out with the IRAM PdBI. IRAM is supported by Institut National des Sciences de l'Univers/CNRS (France), the Max-Planck-Gesellschaft (Germany), and the Instituto Geográfico Nacional (Spain). It was stimulated by discussions held in the context of the European Marie Curie Research Training Network "Constellation" (MRTN-CT2006-035890). We are grateful to the IRAM Director, who awarded us one track of Director's Discretionary Time on the PdBI to confirm the detection of Oph B-11 in the 3.2-mm continuum. We thank F. Gueth and R. Neri for their help and expert advice concerning the interferometric data reduction for this project and M. Pound for useful comments on Oph B-11. The interferometric data used in this paper are archived at IRAM and available upon request from either IRAM or the corresponding author.

Supplementary Materials

www.sciencemag.org/cgi/content/full/337/6090/69/DC1
Supplementary Text
Figs. S1 and S2
References (*33*–*48*)

29 March 2012; accepted 1 June 2012
10.1126/science.1222602

Heralded Entanglement Between Widely Separated Atoms

Julian Hofmann,[1] Michael Krug,[1] Norbert Ortegel,[1] Lea Gérard,[1] Markus Weber,[1]* Wenjamin Rosenfeld,[1,2]* Harald Weinfurter[1,2]

Entanglement is the essential feature of quantum mechanics. Notably, observers of two or more entangled particles will find correlations in their measurement results that cannot be explained by classical statistics. To make it a useful resource, particularly for scalable long-distance quantum communication, the heralded generation of entanglement between distant massive quantum systems is necessary. We report on the creation and analysis of heralded entanglement between spins of two single rubidium-87 atoms trapped independently 20 meters apart. Our results illustrate the viability of an integral resource for quantum information science, as well as for fundamental tests of quantum mechanics.

Entanglement between distant stationary quantum systems will be a key resource for future applications in the field of long-distance quantum communication, such as quantum repeaters (*1*) and quantum networks (*2*). At the same time, it is an essential ingredient for new experiments on the foundations of physics, in particular for a first loophole-free test of Bell's inequality (*3*–*5*). Central to all these applications is the heralded generation of entanglement, i.e., a signal is provided once an entangled pair is successfully prepared.

Until now, (unheralded) entanglement between separated massive quantum objects has been achieved for various systems (*6*, *7*), even over a distance of 21 m (*8*). Heralded entanglement has been demonstrated with cold atomic ensembles (*9*, *10*), single trapped ions (*11*, *12*), and diamond crystals (*13*), albeit over short distances in a single setup only. For the realization of heralded entanglement over long distances, single neutral atoms are promising candidates. In view of future applications, several important milestones have already been demonstrated for such systems: manipulation of atomic quantum registers (*14*), storage of quantum information (*8*, *15*–*17*), fast and highly efficient state analysis (*18*), deterministic quantum gates between nearby trapped atoms via Rydberg blockade (*19*, *20*), and distribution of light-matter entanglement over large distances (*21*).

We report on the preparation and analysis of heralded entanglement between two single ^{87}Rb atoms over a distance of 20 m via entanglement swapping (*22*). The scheme starts with entangling the spin of each of the two atoms with the polarization state of a spontaneously emitted photon (*23*). The photons are guided to a Bell state measurement (BSM) setup where the two-photon polarization state is projected onto an entangled state, thereby providing the heralding signal. In a final step, we evaluate the entanglement between the atomic spins.

Our experimental arrangement (Fig. 1A) consists of two independently operated experiments, here called trap 1 and trap 2 (*24*), which are situated in two laboratories and equipped with their own laser and control systems. In each experiment, we load a single ^{87}Rb atom into an optical dipole trap (*25*). The typical lifetime of a single trapped atom is 5 to 10 s, limited mainly by heating during the experimental process and collisions with background gas. Photons emitted by the atoms are coupled into single-mode optical fibers and guided to the BSM arrangement next to trap 1. The lengths of the optical fibers from trap 1 and trap 2 to the BSM are 5 and 30 m, respectively. To compensate for polarization drifts induced by temperature changes and mechanical stress in the 30-m fiber, an automatic polarization stabilization (*21*) is used. The interferometric BSM arrangement consists of a 50-50 single-mode fiber beam splitter (BS) with polarizing beam splitters (PBSs) in each of the output ports. Additional half- and quarterwave plates allow us to select the measurement basis for the BSM and the atom-photon entanglement measurements. Finally, photons are detected by four avalanche photodiodes (APDs).

First, we verify atom-photon entanglement in each experiment separately. The generation of an entangled atom-photon state starts by preparing the atom in the initial state $5^2S_{1/2}$, $|F = 1, m_F = 0\rangle$ (Fig. 1B) via optical pumping. Then the atom is excited to the state $5^2P_{3/2}$, $|F' = 0, m_{F'} = 0\rangle$ by a short optical pulse (full width at half-maximum pulse length = 21 ns). In the following spontaneous decay, the polarization of a single photon emitted into the collection optics (defining the quantization axis z) is entangled with the atomic spin (*23*), yielding the state

$$|\Psi\rangle_{AP} = \frac{1}{\sqrt{2}}(|\downarrow\rangle_z|L\rangle + |\uparrow\rangle_z|R\rangle)$$

$$= \frac{1}{\sqrt{2}}(|\downarrow\rangle_x|V\rangle + |\uparrow\rangle_x|H\rangle)$$

where $|L\rangle$, $|R\rangle$ denote the left- and right-circular and $|H\rangle$, $|V\rangle$ the horizontal and vertical linear

[1]Fakultät für Physik, Ludwig-Maximilians-Universität München, D-80799 München, Germany. [2]Max-Planck-Institut für Quantenoptik, D-85748 Garching, Germany.

*To whom correspondence should be addressed. E-mail: w.r@lmu.de (W.R.); markusweber@lmu.de (M.W.)

polarization states of the photon. The atomic qubit is defined by the Zeeman states $|m_F = +1\rangle$ and $|m_F = -1\rangle$ of the ground level $5^2S_{1/2}$, F = 1, which we associate with spin orientations $|\uparrow\rangle_z$ and $|\downarrow\rangle_z$, respectively. Preparation and excitation of the atom are repeated until a photon is detected. Taking into account additional cooling periods required to counteract heating of the atom, the preparation and excitation of the atom can be performed 50×10^3 times per second. The overall efficiency for detecting the photon after an excitation in trap 1 (trap 2) is $\eta_1 = 0.9 \times 10^{-3}$ ($\eta_2 = 1.25 \times 10^{-3}$). These numbers include the excitation probability, the collection and coupling efficiencies as well as losses in the optics, and also the quantum efficiency of the photodetectors. Polarization analysis of the single photons is performed with the BSM arrangement, which also serves to monitor fluorescence of the atom inside the trap.

To evaluate atom-photon entanglement, conditioned on the detection of the emitted photon, the internal spin state of the atom is read out (*23*). The detection process consists of a Zeeman state-selective stimulated Raman adiabatic passage (STIRAP) (*26*) with subsequent hyperfine state detection. This process can be considered as a projection of the atom onto the state $\cos(\gamma)|\uparrow\rangle_x + \sin(\gamma)|\downarrow\rangle_x$, where γ is the angle of linear polarization of the STIRAP pulse defining the measurement basis (the angle of the corresponding direction of the atomic spin is 2γ). In atom-photon correlation measurements, we register event numbers $N_{SS'}^{(\gamma,\delta)}$, where $S,S' \in \{|\uparrow\rangle, |\downarrow\rangle\}$ are the eigenstates of the spin of the atom and the photon along their respective measurement directions defined by γ and δ. Figure 2 shows the resulting correlations between atomic spin and photon polarization measurements for both traps separately. In these measurements, the photon was detected in H/V basis ($\delta = 0°$) and in $\pm 45°$ basis ($\delta = 45°$), while the atomic measurement angles α (trap 1) and β (trap 2) were varied between 0° and 180°. The visibilities $V^{(\delta)}$ of the correlation curves obtained by least-squares fits are $V_1^{(0°)} = 0.869 \pm 0.006$, $V_1^{(45°)} = 0.900 \pm 0.006$ for trap 1, and $V_2^{(0°)} = 0.895 \pm 0.004$, $V_2^{(45°)} = 0.901 \pm 0.005$ for trap 2, where the given errors are the expected statistical 1σ deviations. These high visibilities, limited mainly by the quality of the atomic state read-out, demonstrate that atom-photon entanglement is reliably generated and detected with high fidelity in both traps.

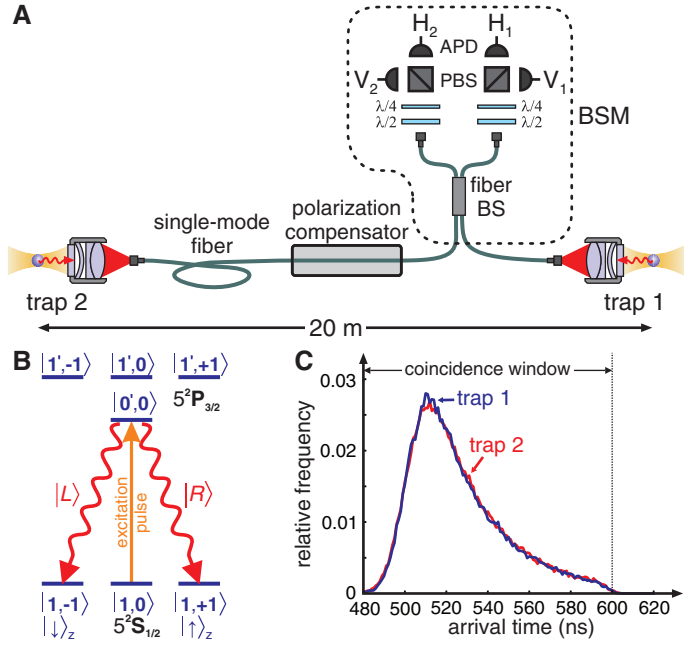

Fig. 1. (**A**) Experimental setting: two independent single atom traps, operated in separate laboratories. Single photons emitted by the atoms interfere on a 50-50 fiber beam splitter (fiber BS) and are detected by APDs behind a polarization analyzer consisting of half- and quarterwave plates ($\lambda/2$ and $\lambda/4$) and PBS. Simultaneous detection of two photons in particular combinations of detectors constitutes a BSM on the photons and heralds the generation of entanglement between the separated atoms. (**B**) Scheme for generation of single photons whose polarization is entangled with the atomic spin. (**C**) Histograms of arrival times of the single photons from trap 1 (blue) and trap 2 (red). The photonic wave packets are overlapped by synchronizing the two excitation procedures to better than 500 ps.

The second crucial condition for preparing a highly entangled state of two trapped atoms is a high-fidelity Bell state measurement of the photons, i.e., projecting them onto maximally entangled states. We use interferometric Bell state analysis based on the Hong-Ou-Mandel effect (*27*). This two-photon detection scheme does not require interferometric stability on a wavelength scale, thereby relaxing the experimental requirements for long-distance quantum communication. In general, at a beam splitter, bunching (antibunching) of two photons in a symmetric (antisymmetric) state enables one to identify Bell states. In our case, a coincidence in detectors H_1V_1 or H_2V_2 (Fig. 1A) signals projection of the photons onto the state $|\Psi^+\rangle_{Ph} = \frac{1}{\sqrt{2}}(|H\rangle|V\rangle + |V\rangle|H\rangle)$, and the coincidences H_1V_2 or H_2V_1 indicate projection onto the state $|\Psi^-\rangle_{Ph} = \frac{1}{\sqrt{2}}(|H\rangle|V\rangle - |V\rangle|H\rangle)$, respectively. The other two symmetric Bell states $|\Phi^\pm\rangle_{Ph} = \frac{1}{\sqrt{2}}(|H\rangle|H\rangle \pm |V\rangle|V\rangle)$ give yet a different result but cannot be distinguished from each other (*28*–*30*). Thus, by detecting one of the four coincidences mentioned above, we project the incoming photons unambiguously on a Bell state, thereby heralding the generation of entanglement between the separated atoms.

The visibility of the two-photon interference, which determines the fidelity of the Bell state measurement, depends crucially on temporal, spatial, and spectral indistinguishability of the arriving photons. Experimentally, the temporal overlap is achieved by synchronizing the two excitation procedures in trap 1 and trap 2 to better than 500 ps, which is far below the lifetime of the excited atomic state of 26.2 ns, and by exactly matching the shapes of the interfering wave packets (Fig. 1C). The single-mode fiber beam splitter guarantees spatial mode overlap of unity. Frequency differences of the emitted photons are minimized by zeroing all relevant fields (*31*). Further reduction of the fidelity of the Bell state measurement arises from two-photon emission by a single atom due to off-resonant excitation of the atom to the $5^2P_{3/2}$, $F' = 1$ level (see Fig. 1B and fig. S1) if the first photon is emitted already within the duration of the excitation pulse. However, owing to the

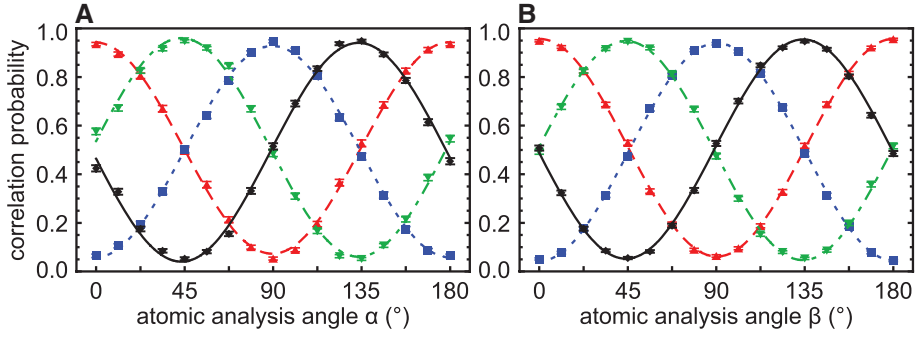

Fig. 2. Atom-photon correlations for trap 1 (**A**) and trap 2 (**B**). The graphs show the measured correlation probabilities $\frac{1}{N}(N_{\uparrow\uparrow}^{(\gamma,0°)} + N_{\downarrow\downarrow}^{(\gamma,0°)})$ (red triangles with dashed lines), $\frac{1}{N}(N_{\uparrow\uparrow}^{(\gamma,45°)} + N_{\downarrow\downarrow}^{(\gamma,45°)})$ (green inverted triangles with dot-dashed lines), and the anticorrelation probabilities $\frac{1}{N}(N_{\uparrow\downarrow}^{(\gamma,0°)} + N_{\downarrow\uparrow}^{(\gamma,0°)})$ (blue squares with dotted lines) $\frac{1}{N}(N_{\uparrow\downarrow}^{(\gamma,45°)} + N_{\downarrow\uparrow}^{(\gamma,45°)})$ (black diamonds with solid lines), $\gamma \in \{\alpha,\beta\}$ as a function of the respective atomic analysis angle. Each point is deduced from $N = 1200$ to 2400 events, where N is the sum over the four possible measurement outcomes.

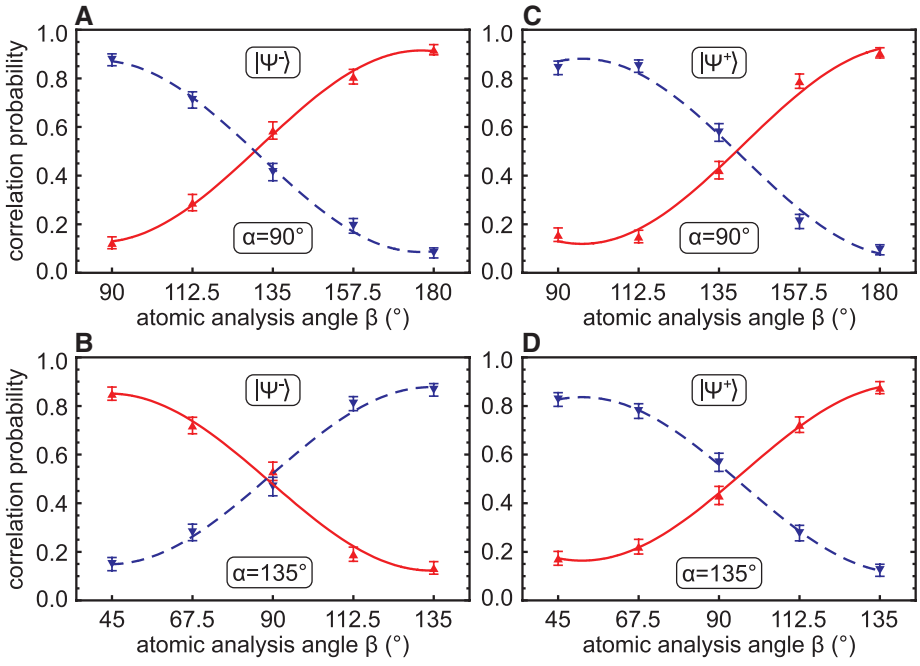

Fig. 3. Atom-atom correlations obtained after Bell state projection of the photons onto state $|\Psi^-\rangle_{Ph}$ (**A** and **B**) and $|\Psi^+\rangle_{Ph}$ (**C** and **D**), respectively. The measured correlation probabilities $\frac{1}{N}(N_{\uparrow\uparrow}^{(\alpha,\beta)} + N_{\downarrow\downarrow}^{(\alpha,\beta)})$ (red triangles with solid lines), and the anticorrelation probabilities $\frac{1}{N}(N_{\uparrow\downarrow}^{(\alpha,\beta)} + N_{\downarrow\uparrow}^{(\alpha,\beta)})$ (blue inverted triangles with dashed lines) are shown for two complementary measurement bases. Each point is deduced from N = 170 to 190 atom-atom events. The overall number of events in this measurement is 3637, acquired within about 107 hours.

structure of the involved atomic levels, with a probability of 78.1% a polarization-entangled state $\frac{1}{\sqrt{2}}(|H\rangle_1|H\rangle_2 + |V\rangle_1|V\rangle_2)$ of the two consecutively emitted photons is formed (*32*). These events are registered as coincidences H_1H_2 and V_1V_2 and do not herald projection onto a Bell state. Reduction of the fidelity is therefore due to the remaining two-photon emissions and to dark counts of the detectors. On the basis of additional calibration measurements, we estimate a fidelity of the Bell state projection of at least 92% (*32*).

By combining all methods described above, we can generate and characterize entanglement between two distant atoms. In each of the two experiments, a single atom is captured and the atom-photon entangling sequences are repeated until two photons are detected within a time window of 120 ns in the BSM arrangement. With a coincidence probability of 0.54×10^{-6} and a repetition rate of 50 kHz, and by taking into account the fraction of time when an atom was present in each of the traps of 0.35, we arrive at an atom-atom entanglement rate of about 1/106 s^{-1}. A valid twofold detection, i.e., registration of $|\Psi^\pm\rangle_{Ph}$, heralds projection of the atoms onto the state $|\Psi^\pm\rangle_{AA} = \frac{1}{\sqrt{2}}(|\uparrow\rangle_x|\downarrow\rangle_x \pm |\downarrow\rangle_x|\uparrow\rangle_x)$. Subsequently, measurements of the atomic states are performed 1.2 μs (trap 1) and 0.95 μs (trap 2) after the coincidence detection (fig. S2). These times are far below the coherence time of the single atomic qubit state of τ_c = 75 μs (*17*) and the coherence time of the entangled atom-atom state, which we expect to be at least $\tau_c/2$, and thus does not limit the quality of our experiment (agreeably, the atom-atom entanglement rate and τ_c need substantial improvement for future quantum repeater scenarios).

To evaluate the atom-atom entanglement, we perform measurements of the atomic spins in two bases. We have chosen analysis angles α = 90° and α = 135°, while β is varied in steps of 22.5° between 90° and 180°, or between 45° and 135°, respectively. The obtained correlations are shown for the detection of the photonic $|\Psi^-\rangle_{Ph}$ state (Fig. 3, A and B) and for the $|\Psi^+\rangle_{Ph}$ state (Fig. 3, C and D). By fitting sinusoidal functions to the data points, we obtain visibilities $V^{(\alpha)}$ of $V_{\Psi^-}^{(90^\circ)} = 0.788 \pm 0.031$, $V_{\Psi^-}^{(135^\circ)} = 0.728 \pm 0.032$ for the $|\Psi^-\rangle_{AA}$ state and $V_{\Psi^+}^{(90^\circ)} = 0.813 \pm 0.030$, $V_{\Psi^+}^{(135^\circ)} = 0.723 \pm 0.034$ for the $|\Psi^+\rangle_{AA}$ state, respectively. For estimation of the fidelity, we assume that the visibility in the third (unmeasured) conjugate basis is equal to the lower of the two measured ones, arriving at $F_{\Psi^-} = 0.811 \pm 0.028$ and $F_{\Psi^+} = 0.815 \pm 0.028$. These numbers prove that in both cases, an entangled state of the two atoms is generated. Moreover, the average visibilities $\overline{V}_{\Psi^\pm} = \frac{1}{2}(V_{\Psi^\pm}^{(90^\circ)} + V_{\Psi^\pm}^{(135^\circ)})$ of $\overline{V}_{\Psi^-} = 0.768 \pm 0.023$ and $\overline{V}_{\Psi^+} = 0.758 \pm 0.023$, respectively, are well above the threshold of 0.707 necessary to violate Bell's inequality.

One of our main goals is to enable a future loophole-free test of Bells inequality (*3*). Inserting the data from the above measurements into $\langle\sigma_\alpha\sigma_\beta\rangle = \frac{1}{N}(N_{\uparrow\uparrow}^{(\alpha,\beta)} + N_{\downarrow\downarrow}^{(\alpha,\beta)} - N_{\uparrow\downarrow}^{(\alpha,\beta)} - N_{\downarrow\uparrow}^{(\alpha,\beta)})$, we evaluated the parameter $S = |\langle\sigma_\alpha\sigma_\beta\rangle + \langle\sigma_{\alpha'}\sigma_\beta\rangle| + |\langle\sigma_\alpha\sigma_{\beta'}\rangle - \langle\sigma_{\alpha'}\sigma_{\beta'}\rangle|$ from the Clauser-Horne-Shimony-Holt-inequality $S \leq 2$, which holds for local-realistic theories (*33*). For the data from Fig. 3, using the settings α = 135°, β = 67.5°; α′ = 135°, β′ = 112.5°; α′ = 90°, β′ = 112.5° together with α′ = 90°, β″ = 157.5° (replacing β = 67.5°), for all four heralding signals we obtain an S value exceeding the limit of 2. Because a measurement result is obtained for each and every heralding signal, the average value of $S = 2.19 \pm 0.09$ for the first time yields definite violation without relying on the fair sampling assumption for a macroscopic distance.

In this experiment, we have demonstrated heralded entanglement between two atoms 20 m apart. It was high enough to violate a Bell inequality, showing its suitability for quantum information applications such as device-independent quantum cryptography (*34*). The design of trap 2 allows rather straightforward extension of the distance between the two traps to at least several hundred meters, limited only by transmission of photons in the optical fiber connection. Two distant entangled atoms form the elementary link of the quantum repeater, enabling efficient long-distance quantum communication. Together with efficient and fast atomic state detection (*18*), this experiment forms the basis for the first loophole-free Bell experiment, answering the long-standing question on whether a local realistic extension of quantum mechanics can be a valid description of nature.

References and Notes

1. H.-J. Briegel, W. Dür, J. I. Cirac, P. Zoller, *Phys. Rev. Lett.* **81**, 5932 (1998).
2. S. J. van Enk, J. I. Cirac, P. Zoller, *Phys. Rev. Lett.* **78**, 4293 (1997).
3. J. F. Clauser, A. Shimony, *Rep. Prog. Phys.* **41**, 1881 (1978).
4. C. Simon, W. T. Irvine, *Phys. Rev. Lett.* **91**, 110405 (2003).
5. W. Rosenfeld *et al.*, *Adv. Sci. Lett.* **2**, 469 (2009).
6. B. Julsgaard, A. Kozhekin, E. S. Polzik, *Nature* **413**, 400 (2001).
7. D. N. Matsukevich *et al.*, *Phys. Rev. Lett.* **96**, 030405 (2006).
8. S. Ritter *et al.*, *Nature* **484**, 195 (2012).
9. C. W. Chou *et al.*, *Science* **316**, 1316 (2007).
10. Z. S. Yuan *et al.*, *Nature* **454**, 1098 (2008).
11. D. L. Moehring *et al.*, *Nature* **449**, 68 (2007).
12. D. N. Matsukevich, P. Maunz, D. L. Moehring, S. Olmschenk, C. Monroe, *Phys. Rev. Lett.* **100**, 150404 (2008).
13. K. C. Lee *et al.*, *Science* **334**, 1253 (2011).
14. D. Schrader *et al.*, *Phys. Rev. Lett.* **93**, 150501 (2004).
15. S. Kuhr *et al.*, *Phys. Rev. Lett.* **91**, 213002 (2003).
16. H. Specht *et al.*, *Nature* **473**, 190 (2011).
17. W. Rosenfeld, J. Volz, M. Weber, H. Weinfurter, *Phys. Rev. A* **84**, 022343 (2011).
18. F. Henkel *et al.*, *Phys. Rev. Lett.* **105**, 253001 (2010).
19. T. Wilk *et al.*, *Phys. Rev. Lett.* **104**, 010502 (2010).
20. L. Isenhower *et al.*, *Phys. Rev. Lett.* **104**, 010503 (2010).
21. W. Rosenfeld *et al.*, *Phys. Rev. Lett.* **101**, 260403 (2008).
22. M. Żukowski, A. Zeilinger, M. A. Horne, A. K. Ekert, *Phys. Rev. Lett.* **71**, 4287 (1993).
23. J. Volz *et al.*, *Phys. Rev. Lett.* **96**, 030404 (2006).

24. M. Weber, J. Volz, K. Saucke, C. Kurtsiefer, H. Weinfurter, *Phys. Rev. A* **73**, 043406 (2006).
25. N. Schlosser, G. Reymond, P. Grangier, *Phys. Rev. Lett.* **89**, 023005 (2002).
26. F. Vewinger, M. Heinz, R. Garcia Fernandez, N. V. Vitanov, K. Bergmann, *Phys. Rev. Lett.* **91**, 213001 (2003).
27. C. K. Hong, Z. Y. Ou, L. Mandel, *Phys. Rev. Lett.* **59**, 2044 (1987).
28. H. Weinfurter, *Europhys. Lett.* **25**, 559 (1994).
29. K. Mattle, H. Weinfurter, P. G. Kwiat, A. Zeilinger, *Phys. Rev. Lett.* **76**, 4656 (1996).
30. S. L. Braunstein, A. Mann, *Phys. Rev. A* **51**, R1727 (1995).
31. W. Rosenfeld *et al.*, *Opt. Spectrosc.* **111**, 535 (2011).
32. Materials and methods are available as supplementary materials on *Science* Online.
33. J. F. Clauser, M. A. Horne, A. Shimony, R. A. Holt, *Phys. Rev. Lett.* **23**, 880 (1969).
34. A. Acín *et al.*, *Phys. Rev. Lett.* **98**, 230501 (2007).

Acknowledgments: We thank A. Deeg, C. Jakob, and C. Kurtsiefer for help during the early stages of the experiment. This work was supported by the European Union Project Q-Essence and the Bundesministerium für Bildung und Forschung Project QuORep. J. H. acknowledges support by Elite Network of Bavaria through the excellence program Quantum Computing, Control and Communication.

Supplementary Materials
www.sciencemag.org/cgi/content/full/337/6090/72/DC1
Materials and Methods
Figs. S1 and S2
Table S1
Reference (*35*)

13 March 2012; accepted 9 May 2012
10.1126/science.1221856

Cavity Cooling Below the Recoil Limit

Matthias Wolke, Julian Klinner, Hans Keßler, Andreas Hemmerich*

Conventional laser cooling relies on repeated electronic excitations by near-resonant light, which constrains its area of application to a selected number of atomic species prepared at moderate particle densities. Optical cavities with sufficiently large Purcell factors allow for laser cooling schemes, avoiding these limitations. Here, we report on an atom-cavity system, combining a Purcell factor above 40 with a cavity bandwidth below the recoil frequency associated with the kinetic energy transfer in a single photon scattering event. This lets us access a yet-unexplored regime of atom-cavity interactions, in which the atomic motion can be manipulated by targeted dissipation with sub-recoil resolution. We demonstrate cavity-induced heating of a Bose-Einstein condensate and subsequent cooling at particle densities and temperatures incompatible with conventional laser cooling.

The discovery of laser cooling has paved the way for fundamental progress in the fields of precision spectroscopy, time and frequency metrology, quantum optics, and quantum gas physics (*1*–*5*). The essential role of repeated electronic excitation constrains the applicability of laser cooling to a limited number of atomic systems, which provide a nearly closed excitation cycle. Reabsorbed spontaneous photons yield stringent limitations with respect to the possible particle densities. The search early on for ways around the unfavorable effects of resonant excitation has led researchers to propose the use of optical cavities, which modify the electromagnetic vacuum. Cooling schemes based on optical cavities promise to be largely unaffected by density limitations and to be applicable to any polarizable matter, including molecules (*6*–*13*). Under certain conditions, cavities may even be used to cool mesoscopic objects as nanoparticles, cantilevers, or thin membranes, which has led to the new field of cavity optomechanics (*14*).

Optical cavities are characterized by two key figures: the rate, η, for scattering into a cavity mode relative to all free-space modes, termed Purcell factor (*15*), and the intracavity field decay rate, $\kappa = 1/2\tau$, which is related to the cavity bandwith, $1/\tau$ (the spectral width of the transmission resonances), and the photon storage time, τ. Two extreme regimes arise. If $\eta > 1$, scattering into modes not supported by the cavity is practically suppressed. If $\hbar\kappa$ (where $\hbar$ is Planck's constant) is smaller than twice the recoil energy, $E_{rec} \equiv \frac{\hbar^2 k^2}{2m}$ (m is the atomic mass, $k \equiv 2\pi/\lambda$, and λ is the optical wavelength), each atom can backscatter only a single photon. The kinetic energy transfer required for backscattering two photons cannot be resonantly supported by the cavity, and hence further backscattering is blocked. Cavity cooling has been experimentally pioneered in the regime $\eta > 1$, $\hbar\kappa \gg E_{rec}$ for large thermal samples by using highly degenerate confocal cavities with moderate finesse and round-trip lengths on the order of cm (*16*, *17*) and with a single or few atoms placed in 100-μm-sized high-finesse single-mode cavities (*9*, *10*). More recently, Bose-Einstein condensates (BECs) were prepared inside such optical cavities in order to study optomechanical interactions and superradiance properties close to zero temperature (*18*–*21*). The regime $\eta < 1$, $\hbar\kappa \simeq 4E_{rec}$ has been addressed in an experiment studying collective atomic recoil lasing and collective scattering in a ring cavity (*22*, *23*). However, the experimentally highly demanding quantum regime,

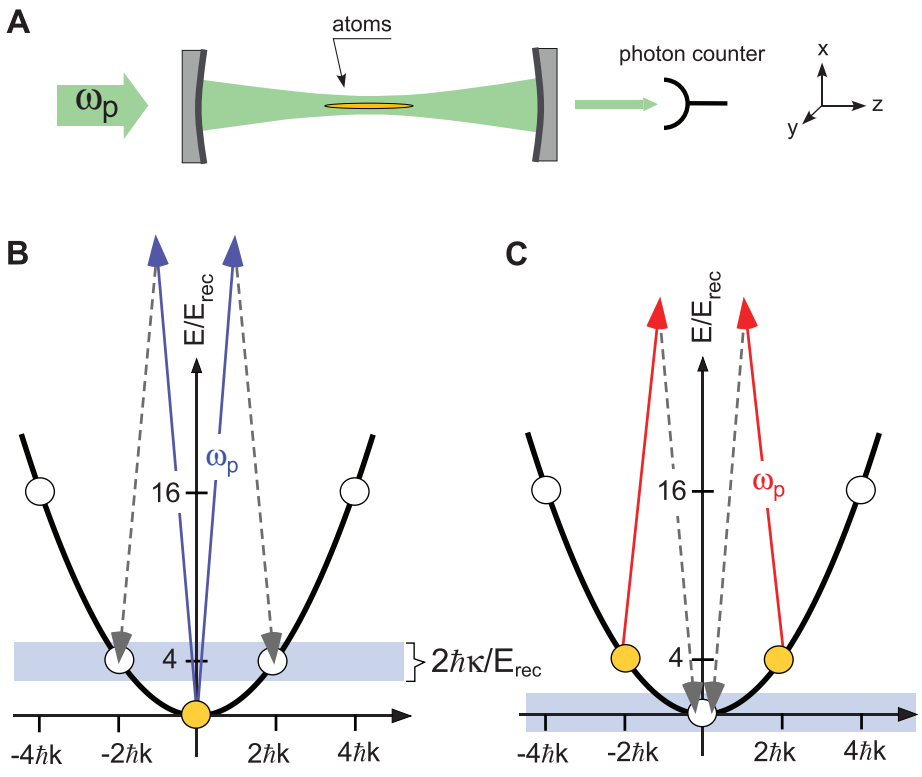

Fig. 1. Experimental scheme and basic processes. (**A**) Sketch of experimental set-up. (**B** and **C**) Cavity-induced heating (B) and cooling (C). The single particle dispersion is sketched by black parabolas. The possible momentum states (multiples of $2\hbar k$) connected by backscattering processes are indicated by solid disks (white if unpopulated, orange if populated). The blue (B) and red (C) solid arrows denote incident photons detuned to the blue and red sides of the cavity resonance, respectively. The dashed gray arrows represent the photons resonantly scattered into the empty cavity. The pale blue horizontal bars indicate the cavity bandwidth.

Institut für Laser-Physik, Universität Hamburg, Luruper Chaussee 149, 22761 Hamburg, Germany.

*To whom correspondence should be addressed. E-mail: hemmerich@physnet.uni-hamburg.de